JOM, Vol. 68, No. 12, 2016
DOI: 10.1007/s11837-016-2112-x

UHV and Ambient Pressure XPS: Potentials for Mg, MgO, and $Mg(OH)_2$ Surface Analysis

ASHLEY R. HEAD[1] and JOACHIM SCHNADT[2,3]

1.—Chemical Sciences Division, Lawrence Berkeley National Laboratory, One Cyclotron Road, Berkeley, CA 94720, USA. 2.—Division of Synchrotron Radiation Research, Department of Physics, Lund University, Box 118, 221 00 Lund, Sweden. 3.—e-mail: joachim.schnadt@sljus.lu.se

The surface sensitivity of x-ray photoelectron spectroscopy (XPS) has positioned the technique as a routine analysis tool for chemical and electronic structure information. Samples ranging from ideal model systems to industrial materials can be analyzed. Instrumentational developments in the past two decades have popularized ambient pressure XPS, with pressures in the tens of mbar now commonplace. Here, we briefly review the technique, including a discussion of developments that allow data collection at higher pressures. We illustrate the information XPS can provide by using examples from the literature, including MgO studies. We hope to illustrate the possibilities of ambient pressure XPS to Mg, MgO, and $Mg(OH)_2$ systems, both in fundamental and applied studies.

INTRODUCTION

X-ray photoelectron spectroscopy (XPS) is a highly mature technique for surface elemental and chemical analysis, based on the photoelectric effect. It has been used frequently in the study of Mg materials, for example to study the oxidation and hydroxylation of Mg and MgO. Conventional XPS, however, suffers from the instrumental necessity of a high vacuum environment ($< 10^{-5}$ mbar), which renders in situ and operando investigations of surface chemical processes, including oxidation and hydroxylation, largely impossible.

This pressure gap between ultrahigh vacuum (UHV) and ambient conditions is exemplified by surface science XPS studies of the native MgO on Mg metal. Under ambient conditions, the surface of MgO is hydroxylated to $Mg(OH)_2$. In order to perform fundamental studies, MgO is easily prepared in vacuum but must be hydroxylated to mirror realistic surface conditions relevant to, e.g., applications. This process is difficult since the room-temperature sticking coefficient of water on MgO(100) in UHV is near zero.[1] MgO(100) can only be hydroxylated above a threshold pressure on the order of 10^{-4} mbar (bulk-like films) to 10^{-6} mbar (bilayer films on a suitable support), and saturation is not reached even at mbar pressures.[2] To properly study the interaction of water with MgO and $Mg(OH)_2$ surfaces in UHV, the sample must instead be cooled. This removes the relevance to applications[3,4] and implies the risk of not overcoming kinetic hindrances of the system, which at realistic temperature and pressure would not play any further role.

The pressure gap can, however, be properly addressed using in situ surface methods such as ambient pressure x-ray photoelectron spectroscopy (APXPS), also known as high-pressure or near-ambient x-ray photoelectron spectroscopy (HPXPS, NAPXPS). The technique allows pressures at the sample in the mbar regime, with a demonstrated maximum pressure of 130 mbar for a standard sample environment[5] and 1 bar for a graphene membrane-based one.[6] Hence, fundamental studies, such as on the hydroxylation of MgO and investigations of $Mg(OH)_2$ relevant to applications, can be conducted in ambient in situ and operando conditions using APXPS.

The objective of this short review is to introduce the Mg community to APXPS. Rather than providing a full account of the method—several excellent reviews outline its details (see, e.g., Refs. 7–13)—we will concentrate on exemplifying some concepts central in XPS, valid also in APXPS. We then discuss the instrumentation of APXPS, before providing a number of examples. Neither of the authors has worked extensively with Mg materials;

(Published online October 3, 2016)

therefore, we primarily provide examples from other areas and make reference to MgO and $Mg(OH)_2$ research to demonstrate how the illustrated concepts find application.

GENERAL ASPECTS OF XPS AND RESEARCH INTO MAGNESIUM OXIDE

Photon sources for photoelectron spectroscopy cover all energies from a few eV up to around 10 keV. Helium discharge lamps have main lines at 21.22 eV and 40.81 eV, and aluminium and magnesium K_α x-ray anodes at 1486.7 eV and 1253.6 eV. In addition, synchrotron radiation sources deliver photons with a tunable energy and play a major role today. The largest majority of available synchrotron beamlines provide vacuum ultraviolet (VUV) and soft x-ray radiation up to 2000 eV, and hence conventional XPS is a VUV and soft x-ray technique. The photoelectric effect then implies that the kinetic energy E_K of the photoelectrons, where

$$E_K = h\upsilon - E_B - \phi, \quad (1)$$

with E_B the binding energy of the electrons in the solid sample, $h\upsilon$ the photon energy, and ϕ the work function of the investigated surface,* typically some tens to hundreds of eV. At such low kinetic energies, the mean free path of the electrons in matter is short: on the order of Ångströms to nanometers in solids and liquids and millimeters in gases at a pressure of 1 mbar. The numbers imply a strong surface sensitivity for solid and liquid samples but lead to difficulties with respect to realistic pressures, which necessitates the APXPS adaptation of XPS (see following section).

The high surface sensitivity of XPS is one of the central aspects in its popularity in surface and materials science, but also the ability to tune between more bulk and more surface-sensitive modes, elemental resolution, chemical resolution from chemical shifts, ease of use and rather straightforward interpretation and semi-quantitative nature of the results, and applicability to essentially any material play an important role. We cannot treat all these aspects here, but limit ourselves to discussion of a few central effects: insulating versus metallic samples and how the method's surface and chemical sensitivity can be employed. For more in-depth treatments, we refer to the excellent review literature of the past decades (e.g. Ref. 14).

*The equation is only valid for metals and the energies refer to the Fermi level of the material. Strictly, for semiconductors and insulators, the proper reference level is the vacuum level, and the work function is omitted from the equation. However, the Fermi level is usable even for sufficiently conductive semiconductors. E_K is measured in the analyzer with a work function that in general is different from that of the sample; therefore, if E_K denotes the actually measured kinetic energy, ϕ is the analyzer (and not the sample) work function. For a properly grounded sample, the Fermi levels of the analyzer and (metallic) sample are aligned apart from a well-defined voltage, and one is only interested in the kinetic energy relative to the measurable Fermi level.

Insulating Samples

Since electrons are detected in XPS, materials with a large band gap are difficult to study. Photoelectrons are not replenished on the timescale of the experiment, leading to excess positive charge on the sample. Outgoing photoelectrons interact with this space charge, which may heavily disturb measured energies and lineshapes to render a spectrum useless. Low-band gap semiconductors such as Si are sufficiently conductive not to pose any problem beyond the difficulty in measuring the Fermi level, the standard reference level according to Eq. 1, which for metallic samples, but not for semiconductors, is easily recognizable as a step edge structure. On properly and regularly calibrated laboratory XPS instruments, the combination of a well-known photon energy with a calibrated analyzer work function implies that the location of the Fermi level is known. The problem is more severe when using a synchrotron x-ray source where the photon energy typically will undergo slight changes over a day. For proper calibration in this case, the Fermi level should be measured for each separate x-ray photoelectron (XP) spectrum, e.g., on a Au foil in good electrical contact with the sample. For somewhat more insulating samples, small charging shifts can occur and the calibration should be done directly before or after measurement of a core/valence level to either another core level or the vacuum level and in the same spot of sample irradiation.[15]

Wide-band gap insulators such as bulk MgO can only be studied with difficulty. If charging is not too strong, reference to the known energy of a core level might be sufficient.[16] Otherwise, a low-energy electron flood gun[17] can be used to replace the depleted charge. The absolute binding energy is then rather arbitrary, but both relative energies and intensities are usable. Thought has then to be given to potential damage to the sample by the electron irradiation, but even the charging itself can give rise to damage, which may be counteracted by the compensation. The method of charge compensation has been used frequently in MgO research (see, e.g., Ref. 18). Alternatively one can use thin, sufficiently conducting MgO films grown on different single crystals.[19,20] Sample heating and concomitant excitation of electrons into the conduction band can also be sufficient to overcome charging.[21]

Surface Sensitivity

The surface sensitive of XPS depends primarily on the kinetic energy $h\nu$ and take-off angle K (Fig. 1a) of the detected electrons with a limited inelastic mean free path λ and thus a relatively short attenuation length Λ in solid matter (Λ is

somewhat shorter than λ since it also contains an elastic contribution[22]). The universal curve of surface science provides an estimate of λ as a function of the electron kinetic energy. From this curve, the minimum mean free path is only a few Å and is observed at a kinetic energy (chosen by the photon energy) of around 50–100 eV. More exact values of λ for specific materials are available (Ref. 23 and references therein).

The intensity I of the electrons varies as $I_0 e^{\frac{-d}{\cos\vartheta}}$, where I_0 is the intensity at the photoemitting atom and d the path length of the electrons to the surface through matter. The exponential behavior implies that for a kinetic energy at the minimum of Λ only the first few nm of the surface contribute to the signal, even in the normal emission case (K = 0°); at grazing emission (K = 80°) virtually only the topmost atomic layer contributes. Variation of the photon energy and/or emission angle provides the opportunity to use XPS for depth profiling in the surface and near-surface region (Fig. 1a). XPS depth profiling has been used in MgO research, e.g., in the determination of the thickness of the surface oxide layer of an oxidized Mg(0001) crystal,[24] localization of hydroxyls after exposure of MgO crystals to water[25] or UHV treatment,[26] and surface segregation of Sr in doped MgO.[27] As a word of caution, intensity changes in XPS can have reasons beyond depth distribution of species, and the surface effect can be completely masked by other phenomena such as photoelectron diffraction.

Chemical Sensitivity

The tabulated[28] approximate binding energies of the core levels of all elements can be used for elemental analysis. The exact energies depend on the chemical environment of the photo-emitting atom, and chemical shifts carry information on the chemical environment and structure, coordination number, oxidation state, etc. In the C 1*s* XP spectra of a monolayer of isonicotinic acid/TiO_2(110) in Fig. 1a,[29] two primary structures can be observed: a larger structure at ~285 eV binding energy and a smaller one at ~289 eV. Based on the observed intensities and expected C 1*s* binding energies of C atoms in heterocycles and carboxylic functional groups,[30] the two features are assigned to photoemissions from the pyridine and carboxyl moieties, respectively. The variation of surface sensitivity by changing the take-off angle leads to a modification of the lineshape of the large peak; the light gray-shaded lower binding energy portion of the peak is decreased more strongly at grazing angles than the darker-shaded higher binding energy part. Noting that the nitrogen-bonded, equivalent carbon atoms

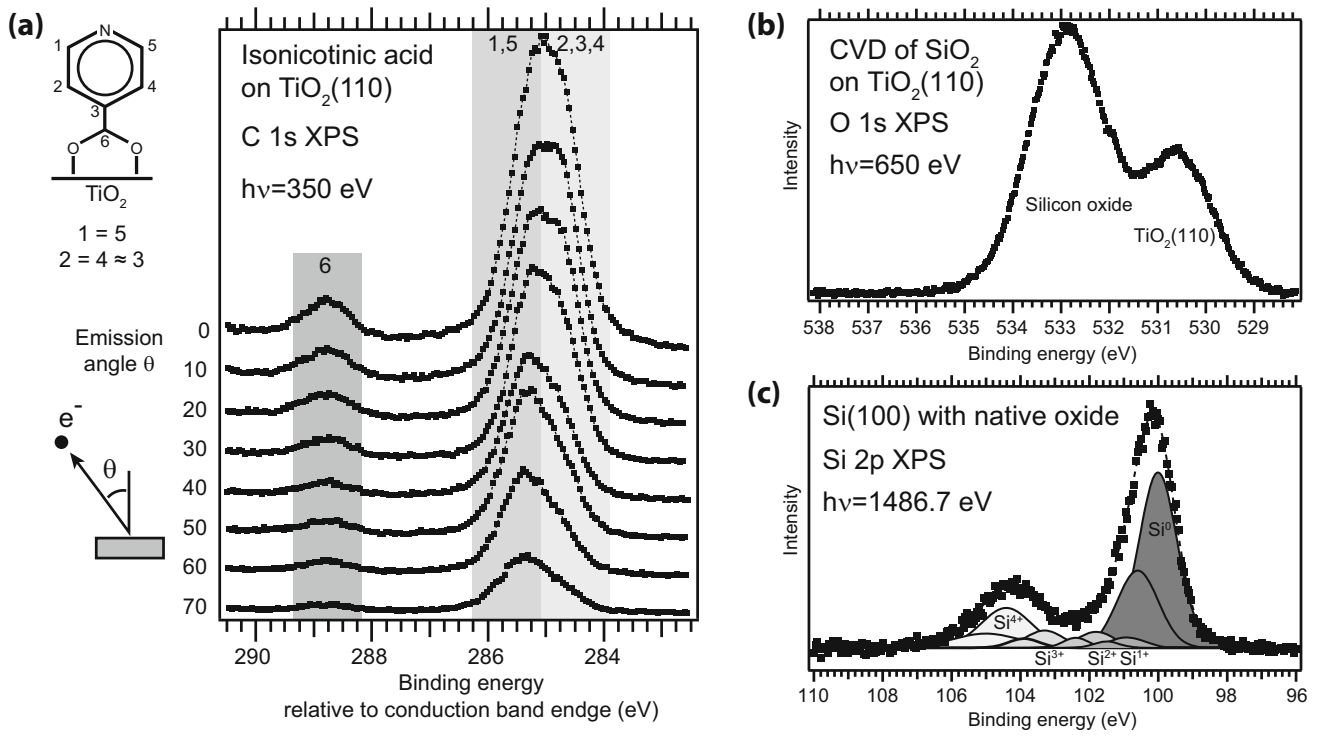

Fig. 1. (a) Emission angle-dependent C 1s XP spectra of a monolayer of isonicotinic acid adsorbed on TiO_2(110). The chemical structure and adsorption geometry of the compound are shown to the left. The chemical equivalence of the different atoms is indicated, and the shaded areas in the spectra correspond to photoemission from these different atoms. Adapted from Ref. 15 with permission from Elsevier. (b, c) Illustration of chemical shifts in XPS: (b) O 1s spectrum of SiO_2 grown on TiO_2(110). (c) Si 2p spectrum of a native oxide-covered Si(100) wafer.

1 and 5 should have a larger binding energy than the other three carbon atoms of the heterocycle (carbon atoms 2, 3, and 4 are chemically similar due to the comparable H and C electronegativities), the changes of the lineshape with angle are easily explained. The molecules stand upright on the surface (as also inferred from other techniques and theory), so atoms 1 and 5 will contribute more strongly than atoms 2, 3, and 4 for very surface sensitive measurements at grazing emission angles. At normal incidence, the reverse applies. Thus, the spectra provide a somewhat more unusual example of depth profiling by XPS.

Two more examples of chemical shifts are shown in Fig. 1b and c. The O 1*s* spectrum in (b) was measured on a layer of SiO_2 grown on TiO_2(110) and exhibits the typical O 1*s* binding energies of the two oxides.[31] They can be distinguished easily, although the formal oxidation states are the same in both materials. In a simplified initial state picture, the shift between the two peaks can be explained by the lower electronegativity of Ti, which donates more electron density to the oxygen atoms than Si. The increased electron density on the O atoms leads to a lower O 1*s* binding energy. Similarly, the Si 2*p* spectrum of the native oxide layer of a Si(100) wafer in Fig. 1c shows well-separated features of bulk Si^0 as well as the substochiometric and stoichiometric silicon oxides (+1, +2, +3, and +4 oxidation states). Each of the oxidation states is represented by a doublet of lines due to the spin-orbit splitting in the final state of the photoemission process as a result of the core photohole.

Chemical shifts in XP spectra of MgO samples have been used to identify Mg oxidation states and the nature of sorbent species. Thus, the Mg 1*s*, 2*s*, and 2*p* binding energies of the Mg^0 oxidation state are ~1.5 eV lower than those of Mg^{2+}.[32,33] In the O 1*s* XP spectra of hydroxlated MgO compounds the hydroxyl O 1*s* line is found at ~2 eV higher binding energy than that of the oxide, and the line of molecular water is another 2 eV higher in binding energy.[34,35] Surface carbonates are intermediate in O 1*s* binding energy between hydroxyls and molecular water.[36] For mixed oxides, one can often distinguish the different contributions: e.g., the O 1*s* line of TiO_2 is ~1.5 eV lower in binding energy than that of MgO.[36]

AMBIENT PRESSURE X-RAY PHOTOELECTRON SPECTROSCOPY

As outlined above, the short electron mean free path in gases at relevant kinetic energies necessitates a high vacuum in conventional XPS. This limitation with respect to in situ and *operando* investigations of surface chemical processes were first overcome in the 1970s, when successful efforts were made to minimize the electron path from the sample to the electron energy analyzer (EEA) through a gas phase surrounding the sample.[37,38] However, though spectra were obtainable, the low count rate had caused the number of in situ XPS experimental setups and studies to be scarce. The combination of modern, intense synchrotron radiation sources with increased EEA transmission[39] popularized APXPS.

Two issues limit the pressure in conventional XPS instruments: high voltage requirements of the EEA and scattering of photoelectrons at higher pressures. A differential pumping scheme between the sample in the measurement chamber and the EEA resolves the issues and permits pressures in the mbar range near the sample and high vacuum conditions in the detector (Fig. 2a).[10] A small aperture close to the sample leads to the first pumping stage where the pressure is about four orders of magnitude lower, while additional pumping stages further lower the pressure before the detector. The signal is maximized by electrostatic focusing onto the apertures between the differential pumping stages.

Gas flow modeling shows that the sample-first aperture distance should be at least twice the aperture diameter to avoid discrepancies between the real and measured pressures.[8,39] A smaller aperture into the differential pumping stage will allow a higher pressure, since the sample can be put closer to the aperture and thus the path of the electrons through the gas is made shorter. For a maximum signal the size of the incoming photon beam should match that of the aperture. The requirement of two aperture diameters can be relaxed somewhat at pressures above around 10 mbar.[40] Other factors that limit the signal, and thus the pressure, are the gas phase photon absorption and the necessary separation of the sample environment from the x-ray/VUV source either by a thin membrane (e.g., Si_3N_4) or differential pumping.[9,10] Gas phase ionizations can overlap ionizations of interest, causing analysis difficulty, but can also be used to detect products or changes in the sample work function.[41]

There are three basic configurations of APXPS measurement chambers as shown in Fig. 2b, c, and d.[10,12] Exposing a sample to a gas in a standard vacuum chamber is the simplest. These chambers typically have large volumes, and a background pressure of the dosed gas remains after the experiment, necessitating a bake-out to restore UHV. A second configuration places the sample in a moveable ambient pressure cell inside a UHV chamber.[12] While this design is more complicated, gases can flow across the sample as opposed to maintaining a static equilibrium. A smaller volume makes for easier cleaning, fast gas exchange, and quick access to UHV and higher pressure conditions. The final configuration uses customizable measurement chambers that are easily placed on the EEA. All of these configurations can combine APXPS with simultaneous measurement of other information including mass spectrometry[12] and cyclic voltammetry.[11,42]

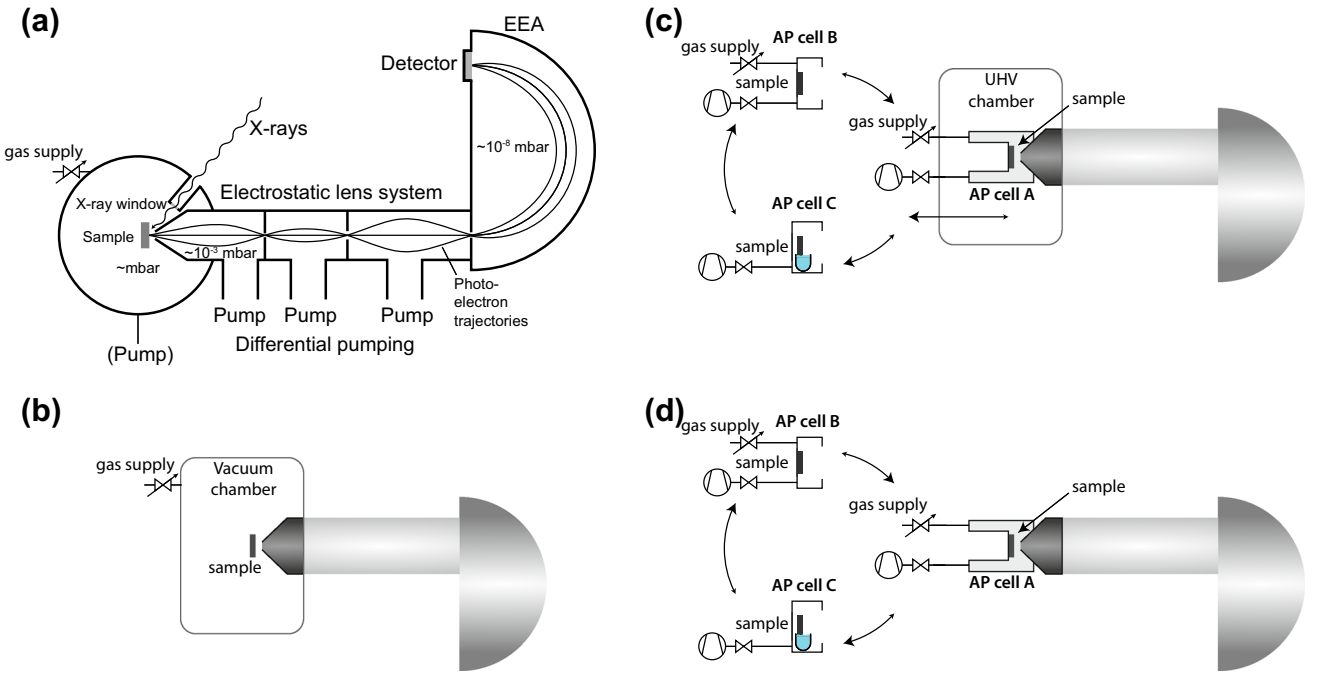

Fig. 2. (a) Differential pumping and electrostatic focusing of the photoelectrons in modern APXPS EEAs. (b–d) Common configurations of measurement chambers. (b–d) are adapted from Ref. 12.

The most common systems studied using APXPS relate to adsorption and reactions at the solid/gas or vapor phase interface. The liquid/vapor interface can be examined using a liquid jet, liquid thin film from vapor condensation, or liquid meniscus above a reservoir of liquid.[11] With higher energy photons, the solid/liquid interface can be studied.[11,43]

APPLICATIONS OF APXPS

The recent availability of APXPS has led to the application of the technique to many fields. For example, the interaction of mineral surfaces,[44] semiconductors,[45] ice,[46] aerosol particles,[47] and amino acids[48] with water has been studied as well as the chemical speciation at the liquid/vapor interface in deliquesced salts[49] and liquid jets.[50] Standing wave spectroscopy has been used to obtain sub-nanometer resolution at the liquid/solid interface in Ni corrosion[51] and ion speciation at the hematite/water interface.[52] Also, surface reactions of electrochemical systems at different biases have been investigated.[42] Below, we highlight two different examples of APXPS studies of light metal systems.

TiO_2 Atomic Layer Deposition

Atomic layer deposition (ALD) is a thin film deposition method for, e.g., metals and metal oxides, nitrides and sulfides,[53] which relies on the surface reactions of two or more alternating gas phase precursors to homogenously coat a surface with precise thickness control, assuming the reactions are complete and self-limiting.[53] Under realistic deposition conditions, the chemistry deviates from the ideal situation, including incomplete precursor reaction, contamination, precursor side reactions, film/substrate mixing, and non-uniform growth. To improve ALD and extend it to other materials, a better understanding of surface chemical mechanisms is required.

An APXPS study of TiO_2 deposition on a $RuO_2(110)$ surface from tetrakis(dimethylamido) titanium (TDMAT) and water has demonstrated the ability to follow electronic structure and chemistry changes in ALD processes under temperature and pressure conditions similar to industrial growth conditions.[54] The ideal ALD model specifies the following surface reactions (* denotes a surface species):

$$\mathrm{Ti(OH)_2^* + Ti[N(CH_3)_2]_4 \rightarrow Ti(O)_2{-}Ti[N(CH_3)_2]_2^* + 2HN(CH_3)_2}$$

$$\mathrm{Ti(O)_2{-}Ti[N(CH_3)_2]_2^* + 2H_2O \rightarrow Ti(OH)_2^* + 2HN(CH_3)_2}$$

Figure 3a and b shows the N 1*s* and Ti 2*p* XP spectra, respectively, during TDMAT and water dosing at ambient pressure. Variation from the ideal chemistry is apparent during the first TDMAT dose: three N surface species, rather than a single, are observed in the spectrum. The majority species are amido ligands, while dimethyl amine and

methyl methyleneimine are assigned to the higher and lower binding energy peaks, respectively. The latter is especially surprising; while transition metal amido complexes decompose to form imines, there has been little evidence of surface-bound imines in ALD processes. The broad Ti 2*p* peak during the TDMAT dosing parallels the multiple N-containing species.

Upon dosing water, further side reactions occur. More dimethyl amine forms and is protonated at higher water pressures (0.1 mbar). Removal of the amido ligand is found to be pressure-dependent, remaining until the water pressure reaches 0.1 mbar. Water does not remove the imine species.

Changes in the spectra are largely cyclic with the alternating doses of the precursors. During the third TDMAT dosing, there is a marked decrease in the amount of imine in the N 1*s* spectra (bottom of Fig. 3a). This decrease is likely due to the changing composition of the surface, which fosters an environment where the imine either does not form or does not adsorb. With completion of three ALD cycles, the Ti 2*p* spectrum looks close to that of bulk TiO_2.

The study also considered basic adsorption and reactivity properties of TDMAT on RuO_2, showing that a multilayer of TDMAT begins to desorb at 40°C. Overlap of the gas phase ionization makes the behavior of the amine difficult to determine. Heat is required to form the imine species, with a small peak appearing around 60°C. Similarly, the Ti^{3+} shoulder appears only after heating.

Overall, the results illustrate that APXPS can be used to examine the surface species of an industrial process at conditions close to those in the application. By conducting these experiments in the cell setup illustrated in Fig. 2c and d, more realistic deposition conditions would be possible to achieve. Studies could also be expanded to, e.g., include depth profiling for comparison of surface and bulk

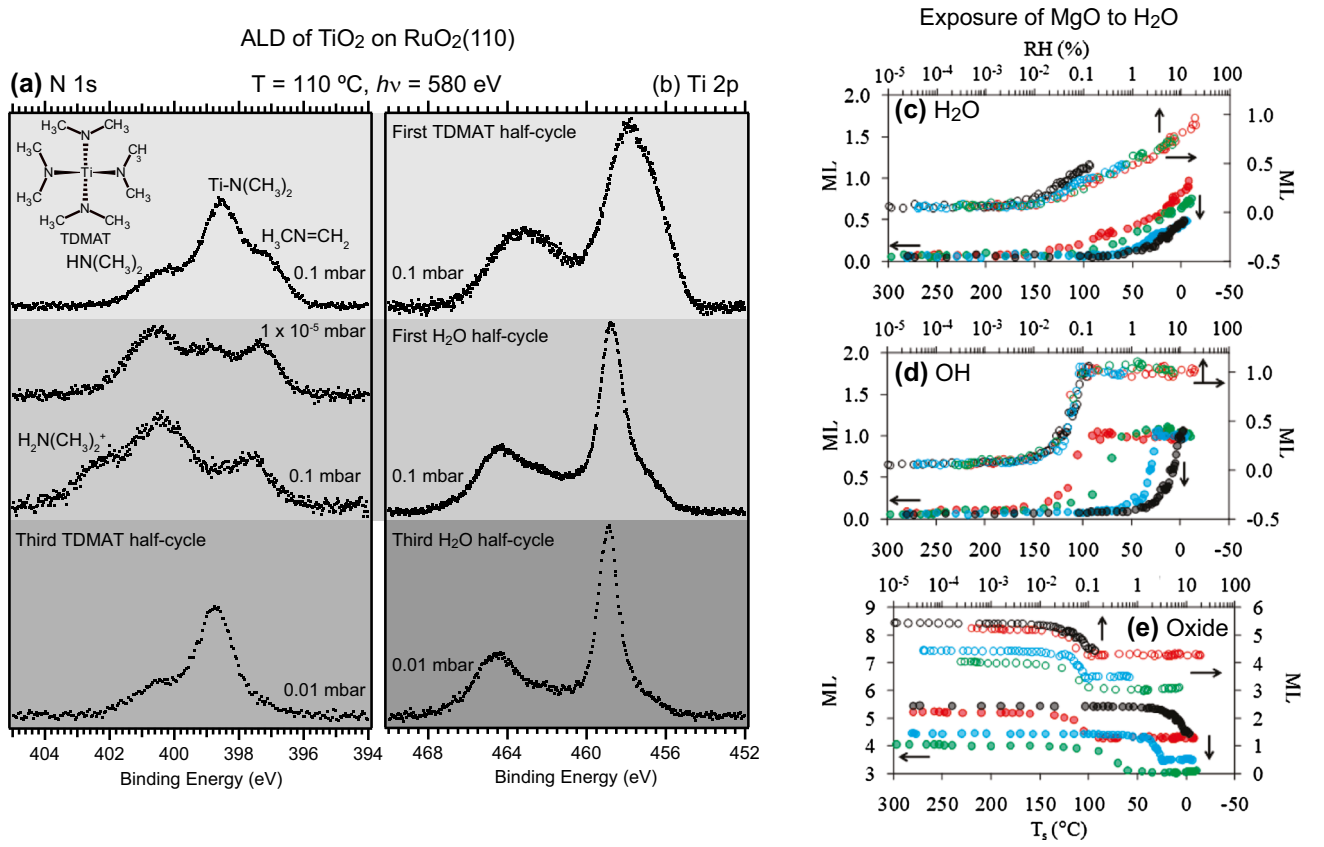

Fig. 3. APXPS examples. (a, b) APXPS of TiO_2 ALD on RuO_2(110). (a) N 1s and (b) Ti 2p XP spectra during the initial TDMAT (cf. inset for the molecular structure) and water half-cycles at the indicated pressures. Different half-cycles are shaded differently. Spectra are normalized to their maximum intensity. (c–e) Surface species coverage of MgO under isobaric conditions of 0.5 (red), 0.15 (green), 0.02 (blue), and 0.005 (black) Torr of water. (c) Molecularly adsorbed water, (d) hydroxyls, and (e) MgO oxide film. The appropriate axis is indicated by the arrows. The relative humidity data are open circles, and the closed circles correspond to the sample temperature axis (T_s). Reprinted with permission from (a, b)[54] and (c–e)[56]; copyright 2016/2011, American Chemical Society.

reactions, monitoring the reaction atmosphere by mass spectrometry, and following chemical structure changes in a time-resolved manner.

MgO Surface Under Ambient Conditions

The MgO(100) surface with its simple rock salt structure is an excellent system for the study of water adsorption, especially since an improved preparation method of Ag-supported bulk-like MgO allows study without extensive sample charging.[34, 55] Changes in the amount of oxide, hydroxide, and water with increasing humidity are easily predicted from the O 1*s* and Ag 3*d* XPS signals and thus hydroxylation is quantified.[34] The hydroxylation can indeed be studied in UHV by exposing the sample to higher pressures of water in a separate chamber connected to UHV instrumentation.[2] However, the behavior of physisorbed water is not accessible as there is no guarantee that the water will remain on the surface in UHV. Therefore, APXPS was used to study the details of surface hydroxylation and molecular water adsorption under isobaric conditions, i.e. at different relative humidities (RHs).[56] Only surface defect sites (~0.08 monolayers) are hydroxylated at RHs < 0.01%, and a small amount of water (~0.07 monolayers) binds to the surface via hydrogen bonds with OH groups. The OH coverage jumps to a saturation of 1 monolayer between 0.01% and 0.1% RH (with the assumption of two OH groups per Mg), accompanied by a gradual increase in water coverage. The splitting of water on five-coordinate terrace sites of the MgO(100) surface is responsible for this increase. Terrace sites have been calculated to be energetically unfavorable sites for water splitting; therefore, an autocatalytic dissociation mechanism is proposed where adsorbed water molecules lower the dissociation energy for a neighboring molecule. The 0.01% RH is the threshold pressure that initiates the dissociation. Upon the completion of a ML of OH groups, molecular water gradually adsorbs on the surface, up to 1 ML at 20% RH. This experiment provides support for DFT calculations predicting the autocatalysis mechanism.[57]

When plotted on a RH scale, OH coverage under isobaric conditions overlap (cf. Fig. 3c, d, and e), indicating an adsorption/desorption surface equilibrium. Thermodynamic parameters of the surface hydroxylation have been calculated from this data.[58] A Clausius–Clapeyron analysis of the data shows that the enthalpy (ΔH^{o}) of the terrace site hydroxylation is -40 kJ mol^{-1} $\pm$ 2 kJ mol^{-1} and the entropy (ΔS^{o}) is -50 kJ mol^{-1} $\pm$ 7 kJ mol^{-1}. From this a Gibbs free energy (ΔG^{o}) of -25 kJ mol^{-1} $\pm$ 1 kJ mol^{-1} was calculated. Kinetic information can also be gleaned from the APXPS data, including the adsorption/desorption equilibrium constants and desorption frequency factor [1.4 ($\pm$1.2) $\times$ 10^{11} s^{-1}]. The electronic structure information gained from APXPS thus provided structural, mechanistic, thermodynamic, and kinetic details in environmental conditions, demonstrating the breadth of possibilities of the technique in the characterization of surface reactions.

CONCLUSION

With this short review, we hope to have demonstrated some of the versatility of APXPS for the investigation of samples in ambient pressure conditions up to 10's of mbar. In relation to studies of the solid/gas or solid/vapor interface, APXPS offers the option of identifying surface and sorbate species which cannot be formed in lower pressure conditions. APXPS makes it possible to study, in real time, chemical reactions driven by the gas phase chemical potential, and accesses valuable information on reaction mechanisms. Improved time resolution, initially down to the second and millisecond timescales, provides the opportunity to identify transitional species which occur only during exposure of a solid sample to a reactant phase. Although not discussed here, the real-time combination and correlation of APXPS with, e.g., mass spectrometry or cyclic voltammetry is extremely powerful for gaining insight into otherwise inaccessible chemical processes. Sample environments previously out of reach for electron spectroscopy studies, such as the solid/liquid and liquid/vapor interfaces, thin film growth reactors and electrochemical cells, are presently becoming standard in APXPS investigations and will further widen the scope of APXPS.

In relationship to Mg research, the hydroxylation process of MgO is now well studied, and the door of opportunity is open for APXPS studies of more complex interactions of $Mg(OH)_2$ with other molecules of relevance to applications. We hope this review can stimulate researchers in the Mg research community to start using the technique.

ACKNOWLEDGEMENTS

We would like to acknowledge our collaborators, Jesper N. Andersen, Hendrik Bluhm, Paul A. Brühwiler, Fabrice Bournel, Barbara Brena, Shilpi Chaudhary, Jean-Jacques Gallet, Niclas Johansson, Jan Knudsen, Juraj Krempaský, Nils Mårtensson, Giorgia Olivieri, Luc Patthey, François Rochet, Joachim Schiessling, Payam Shayesteh, Ming Shi, and Heloïse Tissot, who have all contributed to the data shown.

REFERENCES

1. M.J. Stirniman, C. Huang, R.S. Smith, S.A. Joyce, and B.D. Kay, *J. Chem. Phys.* 105, 1295 (1996).
2. E. Carrasco, M.A. Brown, M. Sterrer, H.-J. Freund, K. Kwapien, M. Sierka, and J. Sauer, *J. Phys. Chem. C* 114, 18207 (2010).
3. M.-C. Wu, C.A. Estrada, J.S. Corneille, and D.W. Goodman, *J. Phys. Chem.* 96, 3982 (1992).
4. D. Ferry, A. Glebov, V. Senz, J. Suzanne, J.P. Roennies, and H. Weiss, *J. Chem. Phys.* 105, 1697 (1996).
5. S. Kaya, H. Ogasawara, L.-Å. Näslund, J.-O. Forsell, H.S. Casalongue, D.J. Miller, and A. Nilsson, *Catal. Today* 205, 101 (2013).
6. J.J. Velasco-Vélez, V. Pfeifer, M. Hävecker, R. Wang, A. Centeno, A. Zurutuza, G. Algara-Siller, E. Stotz, K. Skorupska, D. Teschner, P. Kube, P. Braeuninger-Weimer, S. Hofmann, R. Schlögl, and A. Knop-Gericke, *Rev. Sci. Instrum.* 87, 053121 (2016).
7. M. Salmeron and R. Schlögl, *Surf. Sci. Rep.* 63, 169 (2008).
8. H. Bluhm, *J. Electron Spectrosc. Relat. Phenom.* 177, 71 (2010).
9. A. Knop-Gericke, E. Kleimenov, M. Hävecker, R. Blume, D. Teschner, S. Zafeiratos, R. Schlögl, V.I. Bukhtiyarov, V.V. Kaichev, I.V. Prosvirin, A.I. Nizovskii, H. Bluhm, A. Barinov, P. Dudin, and M. Kiskinova, High-pressure X-ray photoelectron spectroscopy: a tool to investigate heterogeneous catalytic processes. *Advances in Catalysis*, vol. 52, ed. B.C. Gates and H. Knözinger (Burlington: Academic Press, 2009), pp. 213–272.
10. D.E. Starr, Z. Liu, M. Hävecker, A. Knop-Gericke, and H. Bluhm, *Chem. Soc. Rev.* 42, 5833 (2013).
11. E.J. Crumlin, Z. Liu, H. Bluhm, W. Yang, J. Guo, and Z. Hussain, *J. Electron Spectrosc. Relat. Phenom.* 200, 264 (2015).
12. J. Knudsen, J.N. Andersen, and J. Schnadt, *Surf. Sci.* 646, 160 (2015).
13. A.R. Head and H. Bluhm, Ambient pressure X-ray photoelectron spectroscopy. *Elsevier Reference Module in Chemistry, Molecular Sciences and Chemical Engineering*, ed. J. Reedijk (Waltham: Elsevier, 2016).
14. S. Hüfner, *Photoelectron Spectroscopy. Principles and Applications*, 3rd ed. (Berlin: Springer, 2003).
15. J. Schnadt, J.N. O'Shea, L. Patthey, J. Krempaský, N. Mårtensson, and P.A. Brühwiler, *Phys. Rev. B* 67, 235420 (2003).
16. X.D. Peng and M.A. Barteau, *Catal. Lett.* 7, 395 (1990).
17. J. Cazaux, *J. Electron Spectrosc. Relat. Phenom.* 105, 155 (1999).
18. H. Onishi, C. Egawa, T. Aruga, and Y. Iwasawa, *Surf. Sci.* 191, 479 (1987).
19. J. Wollschläger, J. Viernow, C. Tegenkamp, D. Erdös, K.M. Schröder, and H. Pfnür, *Appl. Surf. Sci.* 142, 129 (1999).
20. M.-C. Wu, J.S. Corneille, C.A. Estrada, J.-W. He, and D.W. Goodman, *Chem. Phys. Lett.* 182, 472 (1991).
21. R. Price, T. Eralp-Erden, E. Crumlin, S. Rani, S. Garcia, R. Smith, L. Deacon, C. Euaruksakul, and G. Held, *Top. Catal.* 59, 516 (2016).
22. A. Jablonski and C.J. Powell, *Surf. Sci.* 606, 644 (2012).
23. H. Shinotsuka, S. Tanuma, and C.J. Powell, *Surf. Interface Anal.* 47, 871 (2015).
24. X.D. Peng and M.A. Barteau, *Surf. Sci.* 233, 283 (1990).
25. P. Liu, T. Kendelewicz, G.E. Brown, and G.A. Parks, *Surf. Sci.* 412/413, 287 (1998).
26. V.K. Lazarov, R. Plass, H.-C. Poon, D.K. Saldin, M. Weinter, S.A. Chambers, and M. Gajdardziska-Josifosvska, *Phys. Rev. B* 71, 115434 (2005).
27. L.L. Cao, R.G. Egdell, W.R. Flavell, K.F. Mok, and W.C. Mackrodt, *J. Mater. Chem.* 1, 785 (1991).
28. A. Thompson, D. Attwood, E. Gullikson, M. Howells, K.-J. Kim, J. Kirz, J. Kortright, I. Lindau, Y. Liu, Pi Pianetta, A. Robinson, J. Scofield, J. Underwood, G. Williams, H. Winick, *X-ray Data Booklet* (Lawrence Berkeley National Laboratory, Berkeley, 2009). http://xdb.lbl.gov. Accessed 15 July 2016.
29. J. Schnadt, J.N. O'Shea, L. Patthey, J. Schiessling, J. Krempaský, M. Shi, N. Mårtensson, and P.A. Brühwiler, *Surf. Sci.* 544, 74 (2003).
30. NIST XPS database. http://srdata.nist.gov/xps/. Accessed 15 July 2016.
31. S. Chaudhary, A.R. Head, R. Sánchez-de-Armas, H. Tissot, F. Bournel, L. Montelius, L. Ye, F. Rochet, J.-J. Gallet, B. Brena, and J. Schnadt, *J. Phys. Chem. C* 119, 19149 (2015).
32. J. Lahtinen, J.U. Vaari, A. Talo, A. Vehanen, and P. Hatuojärvi, *Surf. Sci.* 235, 244 (1991).
33. S.J. Splinter, N.S. McIntyre, W.N. Lennard, K. Griffiths, and G. Palumbo, *Surf. Sci.* 292, 130 (1993).
34. J.T. Newberg, D.E. Starr, S. Yamamoto, S. Kaya, T. Kendelewicz, E.R. Mysak, S. Porsgaard, M.B. Salmeron, G.E. Brown, A. Nilsson, and H. Bluhm, *Surf. Sci.* 605, 89 (2011).
35. L.O. Paz-Borbón, A. Hellman, and H. Grönbeck, *J. Phys. Chem. C* 116, 3545 (2012).
36. A. Sasahara, T. Murakami, and M. Tomitori, *J. Phys. Chem. C* 119, 8250 (2015).
37. H. Siegbahn and K. Siegbahn, *J. Electron Spectrosc. Relat. Phenom.* 2, 319 (1973).
38. H. Siegbahn, *J. Phys. Chem.* 89, 897 (1985).
39. D.F. Ogletree, H. Bluhm, G. Lebedev, C.S. Fadley, Z. Hussain, and M. Salmeron, *Rev. Sci. Instrum.* 73, 3872 (2002).
40. M. Kahk, I.J. Villar-Garcia, L. Grechy, P.J.K. Bruce, P.E. Vincent, S.K. Eriksson, H. Rensmo, M. Hahlin, J. Åhlund, M.O.M. Edwards, and D.J. Payne, *J. Electron Spectrosc. Relat. Phenom.* 205, 57 (2015).
41. H. Siegbahn and M. Lundholm, *J. Electron Spectrosc. Relat. Phenom.* 28, 135 (1982).
42. K.A. Stoerzinger, W.T. Hong, E.J. Crumlin, H. Bluhm, and Y. Shao-Horn, *Acc. Chem. Res.* 48, 2976 (2015).
43. S. Axnanda, E.J. Crumlin, B. Mao, S. Rani, R. Chang, P.G. Karlsson, M.O.M. Edwards, M. Lundqvist, R. Moberg, P. Ross, Z. Hussain, and Z. Liu, *Sci. Rep.* 5, 09788 (2015).
44. S. Yamamoto, T. Kendelewicz, J.T. Newberg, G. Ketteler, D.E. Starr, E.R. Mysak, K. Andersson, H. Ogasawara, H. Bluhm, M. Salmeron, G.E. Brown, and A. Nilsson, *J. Phys. Chem. C* 114, 2256 (2010).
45. X. Zhang and S. Ptasinska, *Phys. Chem. Chem. Phys.* 17, 3909 (2015).
46. A. Krepelová, T. Bartels-Rausch, M.A. Brown, H. Bluhm, and M. Ammann, *J. Phys. Chem. A* 117, 401 (2013).
47. E.R. Mysak, D.E. Starr, K.R. Wilson, and H. Bluhm, *Rev. Sci. Instrum.* 81, 016106 (2010).
48. A. Shavorskiy, F. Aksoy, M.E. Grass, Z. Liu, H. Bluhm, and G. Held, *J. Am. Chem. Soc.* 113, 6659 (2011).
49. S. Ghosal, J.C. Hemminger, H. Bluhm, B.S. Mun, E.L.D. Hebenstreit, G. Ketteler, D.F. Ogletree, F.G. Requejo, and M. Salmeron, *Science* 307, 563 (2005).
50. M.A. Brown, R. D'Auria, I.-F.W. Kuo, M.J. Krisch, D.E. Starr, H. Bluhm, D.J. Robias, and J.C. Hemminger, *Phys. Chem. Chem. Phys.* 10, 4778 (2008).
51. O. Karslioglu, S. Mesak, I. Zegkinoglou, A. Shavorskiy, M. Hartl, F. Salmassi, E.M. Gullikson, M.L. Ng, C. Rameshan, B. Rude, D. Bianculli, A.A. Cordones, S. Axnanda, E.J. Crumlin, P.N. Ross, C.M. Schneider, Z. Hussain, Z. Liu, C.S. Fadley, and H. Bluhm, *Faraday Discuss.* 180, 35 (2015).
52. S. Nemsak, A. Shavorskiy, O. Karslioglu, I. Zegkinoglou, A. Rattanachata, C.S. Conlon, A. Keqi, P.K. Greene, E.C. Burks, F. Salmassi, E.M. Gullikson, S.-H. Yang, K. Liu, H. Bluhm, and C.S. Fadley, *Nat. Commun.* 5, 1 (2014).
53. V. Miikkulainen, M. Leskelä, and R.L. Puurunen, *Appl. Phys. Rev.* 113, 021301 (2013).
54. A.R. Head, S. Chaudhary, G. Olivieri, F. Bournel, J.N. Andersen, F. Rochet, J.-J. Gallet, and J. Schnadt, *J. Phys. Chem. C* 120, 243 (2016).
55. D.E. Starr, C. Weis, S. Yamamoto, A. Nilsson, and H. Bluhm, *J. Phys. Chem. C* 113, 7355 (2009).
56. J.T. Newberg, D.E. Starr, S. Yamamoto, S. Kaya, T. Kendelewicz, E.R. Mysak, S. Porsgaard, M.B. Salmeron, G.E. Brown, A. Nilsson, and H. Bluhm, *J. Phys. Chem. C* 115, 12864 (2011).
57. R.S. Alvim, I. Borges Jr., D.G. Costa, and A.A. Leitão, *J. Phys. Chem. C* 116, 738 (2012).
58. J.T. Newberg, *J. Phys. Chem. C* 118, 29187 (2014).